Journal of Solid State Chemistry 181 (2008) 3366–3373

Contents lists available at ScienceDirect

Journal of Solid State Chemistry

journal homepage: www.elsevier.com/locate/jssc

Synthesis, crystal structure and magnetic properties of a new pillared perovskite $La_5Mo_{2.75}V_{1.25}O_{16}$

Farshid Ramezanipour [a,b], Shahab Derakhshan [a,b], John E. Greedan [a,b,*], Lachlan M.D. Cranswick [c]

[a] Department of Chemistry, McMaster University, Hamilton, Ontario, Canada L8S 4M1
[b] Brockhouse Institute for Materials Research, McMaster University, Hamilton, Ontario, Canada L8S 4M1
[c] Canadian Neutron Beam Centre, National Research Council, Chalk River Laboratories, Chalk River, Ontario, Canada K0J 1J0

ARTICLE INFO

Article history:
Received 17 July 2008
Received in revised form
10 September 2008
Accepted 11 September 2008
Available online 2 October 2008

Keywords:
Pillared perovskites
Short-range and long-range magnetic order
Crystal and magnetic structure
Neutron diffraction

ABSTRACT

A new pillared perovskite compound $La_5Mo_{2.76(4)}V_{1.25(4)}O_{16}$, has been synthesized by solid-state reaction and its crystal structure has been characterized using powder X-ray and neutron diffraction. The magnetic properties of this compound have been investigated using SQUID magnetometry, and the magnetic structure has been studied using neutron diffraction data. A theoretical calculation of relative strengths of spin interactions among different magnetic ions and through different pathways has been performed using extended Hückel, spin dimer analysis. The crystal structure of this material contains perovskite-type layers that are connected through edge-sharing dimeric units of octahedra. The structure is described in space group $C2/m$ with unit cell parameters $a = 7.931(2)$ Å, $b = 7.913(2)$ Å, $c = 10.346(5)$ Å and $\beta = 95.096(5)^\circ$. The material shows both short-range ferrimagnetic correlations from ~200 to 110 K and long-range antiferromagnetic order below T_c~100 K. The magnetic structure was investigated by neutron diffraction and is described by $k = (0\,0\,\frac{1}{2})$ as for other pillared perovskites. It consists of a ferrimagnetic arrangement of Mo and V within the layers that are coupled antiferromagnetically between layers. This is the first magnetic structure determination for any Mo-based pillared perovskite.

1. Introduction

Materials with perovskite-related structures have been attracting a great deal of interest over the past decades. Observation of interesting physical properties such as superconductivity, metal–insulator transitions and colossal magnetoresistance in perovskite-type structures with possible applications in magnetic memory devices and in detection of magnetic fields has inspired a large number of studies [1–7]. Starting with the synthesis of $La_5Mo_4O_{16}$ in 1983 [8] via fused salt electrolysis and the report of its crystal structure 10 years later [9] a new family of perovskite-related materials was introduced (Fig. 1), consisting of a quasi-two-dimensional structure with perovskite-type layers separated by dimeric units of edge-sharing octahedra (hatched grey). Note that there are two types of octahedra in a corner-sharing layer: the $M(1)O_6$ octahedron (grey) shares only four equatorial corners with the other octahedra, and its apical corners are not shared. The second octahedron, $M(2)O_6$ (black), shares all six corners: the two apical corners are shared with the pillaring units located on the top and below, and the four equatorial corners are shared with the other octahedra within the perovskite-type layer. The two types of octahedra are arranged so that $M(1)O_6$ has only $M(2)O_6$ neighbors and vice versa. For several years this material was the unique example of this structure type, until two groups of compounds with the formulae $La_5Re_3MO_{16}$ (M = Mn, Mg, Fe, Co, Ni) and $La_5Mo_{4-x}M_xO_{16}$ (M = Mn, Mg, Fe, Co and x~0.75) were reported [10–12], followed by another compound, $La_5Os_3MnO_{16}$ [13]. In these cases Re^{5+} and Os^{5+} substitute for Mo^{4+} in both the dimers and the perovskite layers on the $M1$ site and divalent 3d transition metal ions occupy the $M2$ site. These materials exhibit interesting magnetic properties. Short metal–metal distances within the dimeric units provide evidence for multiple metal–-metal bonding. Due to the long separation (~10 Å) of the perovskite layers by the pillaring, diamagnetic, dimeric units, one may expect to see a two-dimensional magnetic correlations in these materials, with only weak interaction between the layers. However, detailed magnetic studies of these compounds showed long-range magnetic order at temperatures up to 193 K [10,12–18]. Neutron diffraction studies of $La_5Re_3MnO_{16}$ for example showed an antiferromagnetic coupling of ferrimagnetic layers (Re↓ Mn↑) resulting in a three-dimensional magnetic structure below 162 K [15].

It is of interest to extend the crystal chemistry of this new perovskite-related family to include other 3d series transition elements, especially the so-called "early" 3d elements.

* Corresponding author at: Department of Chemistry, McMaster University, Hamilton, Ontario, Canada L8S 4M1. Fax: +1 905 521 2773.
E-mail address: greedan@mcmaster.ca (J.E. Greedan).

0022-4596/$ - see front matter © 2008 Published by Elsevier Inc.
doi:10.1016/j.jssc.2008.09.012

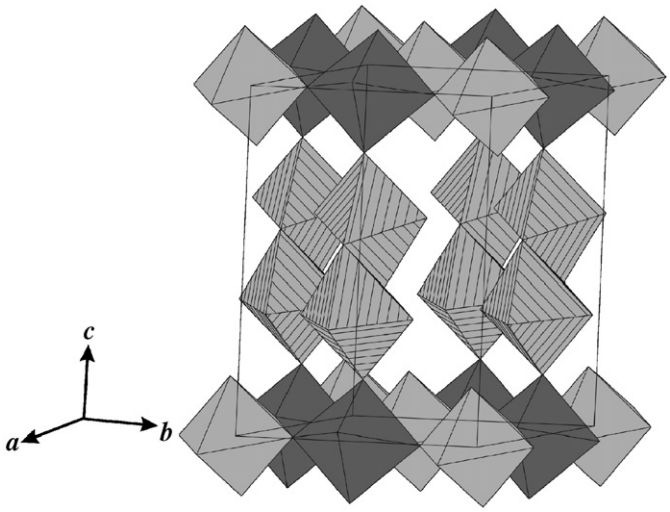

Fig. 1. Crystal structure of a pillared perovskite. The octahedral environments of distinct atomic positions are shown with different shadings. The perovskite layers contain two octahedral sites, *M*1 (grey) and *M*2 (black), which are pillared through corner sharing at *M*2 by edge-sharing dimeric units shown in grey with hatching.

Major synthetic difficulties are associated with these materials, especially the original molybdenum-based series. For example $La_5Mo_4O_{16}$ has been prepared only by molten salt electrolysis. Some members of the $La_5Mo_{4-x}M_xO_{16}$ series can be synthesized by standard solid-state methods but generally not as single-phase products [11]. Here the synthesis, crystal structure and magnetic properties of a new molybdenum-based pillared perovskite containing V^{4+} with the formula $La_5Mo_{2.76(4)}V_{1.25(4)}O_{16}$ is reported using standard solid-state methods. Sufficient material was produced in this manner to permit a neutron diffraction study of the magnetic structure for the first time for any Mo-based pillared perovskite.

2. Experimental section

2.1. Synthesis

A large variety of different synthetic conditions were examined, and a compound, which later proved to be $La_5Mo_{2.76(4)}V_{1.25(4)}O_{16}$ was finally prepared using La_2O_3 (99.99% Alfa Aesar), MoO_2 (99.9% CERAC), V_2O_5 (99.6% Aldrich) and V_2O_3 (prepared in the lab by reduction of VO_2 99.5% CERAC) as starting materials. La_2O_3 was pre-fired at 1000 °C over night before being used in the experiment. Stoichiometric amounts of the reactant powders were weighed, ground together, pressed into a pellet, wrapped in a platinum sheet and sealed in a silica tube under the vacuum ($\sim 10^{-3}$ Pa). The reaction was completed in 24 h at a temperature of 950 °C.

Initially, a Mo:V ratio of 3:1 (in the form of MoO_2 and V_2O_5) was used in the expectation that the low melting point of V_2O_5 would facilitate the solid-state reaction at relatively low temperatures and that the redox couple, $Mo^{4+}/V^{5+} = Mo^{5+}/V^{4+}$ might be operative. The molar ratio of La_2O_3:MoO_2:V_2O_5 used for the experiment was 2.5:3:0.5. However, a large amount of a side product, identified as $La_{2.4}Mo_{1.6}O_8$ [19] with a disordered fluorite structure and Mo oxidation state of +5.5 always appeared along with a majority phase with the pillared perovskite structure. Thus, additional vanadium oxide in the form of V_2O_3 was added to reduce molybdenum to the desired oxidation states (4+ and 5+), and to form the target V-containing material instead of a purely Mo-containing phase. Different trial amounts of excess V, in form of V_2O_3 (and by keeping the above-mentioned ratio for the other reactants), were added and finally 50% excess by mole of vanadium resulted in the desired pillared perovskite compound along with a small amount of an unidentified side product. Structural analysis of the obtained pillared perovskite compound, to be discussed later, showed the actual formula to be $La_5Mo_{2.76(4)}V_{1.25(4)}O_{16}$. Therefore, another experiment was tried using a Mo:V ratio of 2.76(4):1.25(4), that still resulted in formation of a large amount of the side product $La_{2.4}Mo_{1.6}O_8$[19] along with the pillared perovskite compound. Accordingly, the aforementioned procedure with excess of V (V_2O_3) seems to be the best reaction condition.

2.2. X-ray and neutron diffraction

X-ray powder diffraction data was obtained using a PANalytical X'Pert Pro MPD diffractometer with a linear X'Celerator detector. Cu$K\alpha_1$ radiation ($\lambda = 1.54056$ Å) in the 2θ range of 10–110° with a 2θ step interval of 0.0084° was used for data collection. Powder neutron diffraction measurements were performed on the C2 diffractometer at the Canadian Neutron Beam Centre at Chalk River, Ontario. The data were collected at three different temperatures, 3.8, 110.2 and 300 K. Two different wavelengths were used at 3.8 and 300 K with the same step size of 0.100°. The wavelength 1.33037 Å was used to collect data within the 2θ range of 35–115°, and the wavelength 2.37150 Å was applied to obtain data in the 2θ range of 5–85°. The number of Bragg reflections and profile points contained in the short wavelength dataset was 689/673 and 69/582 for the long wavelength dataset.

2.3. Magnetic property measurements

Magnetic data were collected on a Quantum Design MPMS SQUID magnetometer. The zero-field cooled and field cooled (ZFC/FC) magnetic susceptibility from 5 to 300 K and isothermal magnetization data from 0 to 5.5 T were obtained on a powder sample in a gelatin capsule. Diamagnetic corrections of 20×10^{-6} (La^{3+}), 17×10^{-6} (Mo^{4+}), 12×10^{-6} (Mo^{5+}), 7×10^{-6} (V^{4+}) and 12×10^{-6} emu/mol (O^{2-}) were made to the susceptibility data [20].

2.4. Theoretical calculations: spin dimer analyses

A computational estimation of relative strengths of spin interactions among different magnetic ions and through different pathways was obtained using extended Hückel, spin dimer analysis [21]. The strengths of spin interaction manifested in the exchange constant *J* are related to the hopping energies among different magnetic sites, Δe, as well as the electron correlation energy, *U*, resulting from accommodation of two electrons within the same orbital. These quantities are related through the formula

$$J = -2\frac{(\Delta e)^2}{U} \quad (1)$$

when comparing *J* values of different interaction pathways, the correlation energy *U* is constant and therefore the difference in the Δe value determines the significance of a particular spin interaction relative to the other possible pathways.

In these computations different interaction pathways among two *M*1 sites (Mo-rich sites), two *M*2 sites (V-rich sites), as well as an *M*1 and an *M*2 site within a perovskite-type layer were examined, and the values of the intersite hopping energy, Δe, were acquired by employing the CAESAR package [22]. Fig. 2 shows a

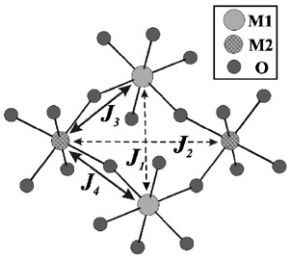

Fig. 2. Spin interactions between magnetic ions within a corner-sharing layer. The solid and dashed arrows represent strong and weak spin interactions, respectively.

Table 1
The values for the ζ_i coefficients and valence shell ionization potentials H_{ii} of the STO's employed for the spin dimer calculations

Atom	Orbital	H_{ii} (eV)	ζ_i	C	ζ_i'	C'
O	2*s*	−32.3000	2.688	0.7076	1.675	0.3745
O	2*p*	−14.8000	3.694	0.3322	1.659	0.7448
Mo	4*s*	−8.3400	1.955	1.0000		
Mo	4*p*	−5.2400	1.360	1.0000		
Mo	4*d*	−10.5000	3.954	0.4930	2.047	0.6458
V	3*s*	−8.8100	1.6970	1.00000		
V	3*p*	−5.5200	1.2600	1.00000		
V	3*d*	−11.0000	5.0520	0.37380	2.173	0.7456

schematic representation of four different spin interactions within a perovskite-type layer. Also the values of valence shell ionization potential H_{ii}, and the ζ_i and ζ_i' coefficients of double zeta Slater-type orbitals applied in the calculations [23,24] are tabulated in Table 1.

3. Results and discussion

3.1. Crystal structure

The crystal structure of $La_5Mo_{2.76(4)}V_{1.25(4)}O_{16}$ was characterized using both X-ray and neutron diffraction data. Data were contaminated by a small amount of an unidentified side product whose peaks were excluded from the diffraction pattern for the final refinement. The Rietveld refinement was performed using the FullProf program [25], employing WinPLOTR [26]. The non-standard space group $C\bar{1}$ has been previously reported for pillared perovskite compounds [10–13], based on Re or Os, although the space group of the original member of this family, $La_5Mo_4O_{16}$, was reported to be $C2/m$ [9]. In fact, the refined cell constants of the Re and Os materials are metrically triclinic while those for $La_5Mo_4O_{16}$ are metrically monoclinic. On the other hand, cell constants for the substituted molybdenum phase, $La_5Mo_{3.31}Co_{0.69}O_{15.8}$, are also metrically monoclinic but the single-crystal X-ray data were refined in $C\bar{1}$ due to poor averaging of equivalent reflections in $C2/m$. Lacking single-crystal X-ray data it is impossible to make a definitive choice here. Thus, the X-ray and neutron diffraction data were refined in both space groups. The refinement in $C\bar{1}$ resulted in unit cell parameters that were metrically very close to those of a monoclinic cell with $\alpha = 89.989(17)^\circ$ and $\gamma = 90.065(16)^\circ$. A full refinement in $C\bar{1}$, using 70 parameters, gave a somewhat better set of agreement indices than with $C2/m$, using 59 parameters, but the derived interatomic distances were not significantly different between the two cases. Thus, we report here only the results for $C2/m$.

An initial refinement was performed on X-ray diffraction data to obtain unit cell parameters and atomic positions for the metal sites to be used for the refinement of the neutron diffraction pattern. These results are shown in Fig. 3 (top) where the impurity reflections are indicated. While the identity of the phase or phases involved could not be determined, the relative intensities suggest an impurity level of ~5–10%. The sensitivity of neutron diffraction to oxygen was a key factor that provided accurate atomic positions, as well as acceptable displacement factors for the oxygen atoms. The large difference between the scattering lengths of Mo and V is another useful feature, as V is nearly invisible to neutrons with a scattering length of −0.3824(12) fm compared to 6.715(20) fm for Mo. Fig. 3 (bottom) shows the observed, calculated and difference profiles for the long wavelength neutron data ($\lambda = 2.37150$ Å), as well as the short wavelength neutron data ($\lambda = 1.33037$ Å).

The initial refinement was based on a 1:1 ratio of Mo:V in the two special positions, *M*1 and *M*2, within a perovskite layer, with Mo positioned at *M*1. The abnormal behavior of the displacement factors of these metal sites in both X-ray and neutron data signaled the possibility of some mixing between Mo and V. This hypothesis was then verified by the refinement of the site occupancies that indicated mixing predominantly on the *M*1 site. Further refinement of site occupancies to reach convergence revealed the ratio of Mo:V at the *M*1 site to be 0.76(4):0.25(4). There was at most a few percent of Mo on the *M*2 site but this was not refined and was taken as fully occupied by V. Essentially the same results were obtained from refinement of the X-ray diffraction data.

A summary of the final refinement results obtained from simultaneous refinement of short and long wavelength neutron data is given in Table 2.

Table 3 shows a list of the atomic positions, site occupancies and the thermal displacement factors.

It is of course of great interest to assign oxidation states to the metal ions in the various sites in the pillared perovskite structure. For the Mo-based series it is reasonable to place $Mo^{4+}(4d^2)$ ions in the dimeric edge-sharing octahedra that connect layers of corner-sharing octahedra. The Mo–Mo distance within the dimers, Mo1–Mo1, is very short, 2.46(2) Å, in this case, and consistent with a Mo–Mo double bond. This value falls within the range found for corresponding intra-dimer distances in $La_5Mo_4O_{16}$, 2.406(1) Å and $La_5Mo_{3.31}Co_{0.69}O_{15.8}$, 2.4920(5) Å [9,11]. The constraints imposed by the edge sharing of two octahedra as well as the corner sharing between Mo_2O_{10} units and perovskite-type layers account for the significant distortion in these pillaring units. Bond distances range from Mo–O1 = 1.901(12) Å to Mo1–O4 = 2.30(2) Å and the O–Mo–O angles vary from 87.1(17)° to 102.6(12)°.

Now, concerning the two sites within the perovskite layers, *M*1 at (000) and *M*2 at (0.500), the formal charges must sum to +9 if full occupancy of the La and O sites is assumed. There are 0.75 Mo ions and 1.25 V ions distributed over these sites. If these are solely Mo^{5+} and V^{4+}, the charge sum is +8.75 which implies either some admixture of Mo^{6+} or V^{5+} or an O^{2-} deficiency. The average *M*1–O distance is 1.99(2) Å and that for *M*2–O is 1.97(2) Å, which are not significantly different. This is in accord with the very similar radii of Mo^{5+} (0.61 Å) and V^{4+} (0.58 Å) and the intersite mixing. The occupation of the *M*1 site refined to ~0.75 Mo and ~0.25 V and with O^{2-} (1.38 Å) the expected *M*1–O distance is 1.98 Å, which is in reasonable agreement with the observed. Full occupation of *M*2 by V^{4+} leads to an expected distance of 1.96 Å. Note that an O^{2-} deficiency of only 0.78% would provide charge balance. Such was claimed for $La_5Mo_{3.31}Co_{0.69}O_{15.8}$ from refinement of X-ray single-crystal data. Attempts to investigate this possibility by refinement of the occupation rates of the oxygen sites were inconclusive.

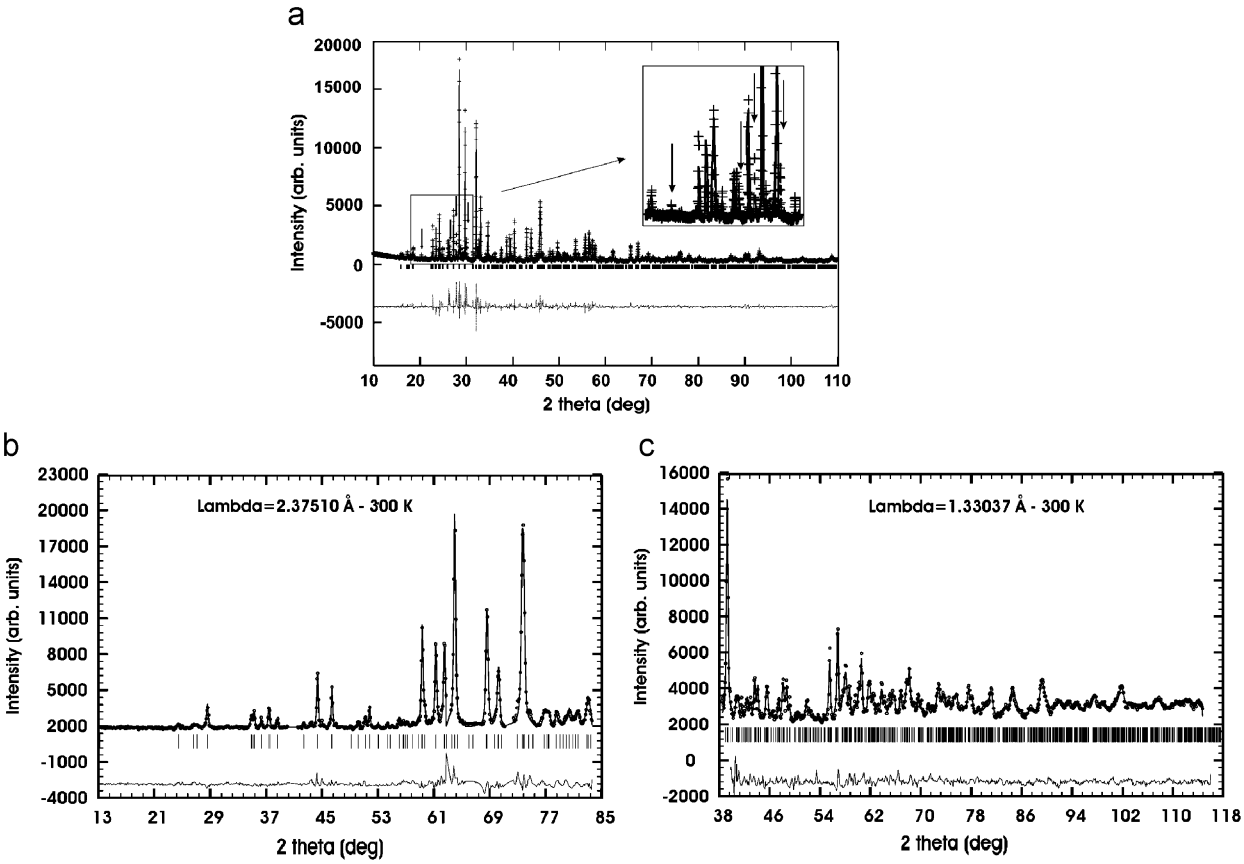

Fig. 3. (a) Rietveld refinement of powder X-ray diffraction data with $\lambda = 1.54056$ Å at room temperature. The main impurity peaks are shown by arrows in the inset that magnifies the X-ray pattern in 2θ range of 18–31.5°. (b) Rietveld refinement of neutron diffraction data with $\lambda = 2.37150$ and 1.33037 Å. The impurity peaks are omitted for final refinement. The black dots are the data, the solid line the model, the vertical tic marks locate Bragg peak positions and the lower line is the difference plot.

Table 2
The final refinement results for $La_5Mo_{2.76(4)}V_{1.25(4)}O_{16}$ neutron diffraction data at 300 K

Space group	$C2/m$
Lattice parameters	$a = 7.931(2)$ Å $b = 7.913(2)$ Å $c = 10.346(5)$ Å $\beta = 95.096(5)°$
Z	2
Agreement factors	R_p (1.33037 Å) = 0.038 R_p (2.37150 Å) = 0.048 R_{wp} (1.33037 Å) = 0.051 R_{wp} (2.37150 Å) = 0.066 R_B (1.33037 Å) = 0.063 R_B (2.37150 Å) = 0.098

Table 3
The atomic coordinates, site occupancies and displacement factors for $La_5Mo_{2.76(4)}V_{1.25(4)}O_{16}$ at 300 K

Atom	x	y	z	Occupancy	B_{iso} (Å^2)
La1	0.2755(12)	0.2483(11)	0.1987(9)	1	0.65(20)
La2	0.0	0.0	0.5	1	1.2(4)
Mo1	0.567(2)	0.0	0.3974(15)	1	0.9(3)
Mo2	0	0	0	0.76(4)	1.1(6)
V2	0	0	0	0.25(4)	1.1(6)
V1	0	0.5	0	1	0.5
O1	0.0385(15)	0.2656(15)	0.3616(10)	1	0.1(2)
O2	0.287(3)	0.5	0.329(2)	1	0.8(4)
O3	0.315(3)	0.0	0.434(2)	1	1.0(3)
O4	0.465(2)	0.0	0.1818(16)	1	0.1(4)
O5	0.068(2)	0.0	0.1748(17)	1	0.3(4)
O6	0.044(3)	0.255(4)	0.004(3)	0.5	1.3(6)
O7	0.249(3)	0.959(3)	0.961(2)	0.5	0.6(5)

The bond valence sum calculations [27,28] give 5.0 for Mo2, 3.6 for V1, and 3.6 for V2, which are close to the expected values of 5 and 4 for Mo and V, respectively, in the perovskite layer. However, it may be problematic to apply this approach to sites for which metal–metal bonding is important as with the Mo1 here. This may explain the large BVS value of 4.7 obtained for Mo1. Given the very short Mo1–Mo1 distance found here and in all other Mo-based pillared perovskites, the only reasonable oxidation state assignment for this site is +4. Core level spectroscopic measurements are planned to probe the distribution of metal oxidation states in this material. As well, note that the $M1$–O octahedron shows a pronounced psuedo-tetragonal compression (Table 4). The Mo2–O5 distance is only 1.841(17) Å, compared to the other two distances at 2.05(3) and 2.08(2) Å. The O5 atom is not bonded to the pillaring dimeric group. A similar distortion is also seen in $La_5Mo_4O_{16}$ and $La_5Mo_{3.31}Co_{0.69}O_{15.8}$ and one of a slightly smaller magnitude exits at the Re layer site in the $La_5Re_3MO_{16}$ series. Finally, given the very small differences in radii and formal charge between Mo^{5+} and V^{4+}, the strong preference of Mo^{5+} for the $M1$ site is remarkable.

3.2. Magnetic properties

Magnetic susceptibility data in the range of 2–300 K, are shown in Fig. 4. The data are dominated by a fairly sharp maximum at ~110 K and a ZFC/FC divergence is seen below the maximum. These data are similar to those obtained for many

Table 4
Selected bond lengths (Å) and angles (deg) for $La_5Mo_{2.76(4)}V_{1.25(4)}O_{16}$ at 300 K

Mo1–O1	1.901(12) × 2
Mo1–O2	1.94(3)
Mo1–O3	1.90(3)
Mo1–O3	2.07(3)
Mo1–O4	2.30(2)
Mo1–Mo1	2.46(2)
Mo2(V2)–O5	1.841(17) × 2
Mo2(V2)–O6	2.05(3) × 2
Mo2(V2)–O7	2.08(2) × 2
V1–O4	1.925(17) × 2
V1–O6	1.97(3) × 2
V1–O7	2.02(2) × 2
O1–Mo1–O1	154.7(11)
O1–Mo1–O2	91.4(13) × 2
O1–Mo1–O3	102.6(12)
O2–Mo1–O3	87.1(17)

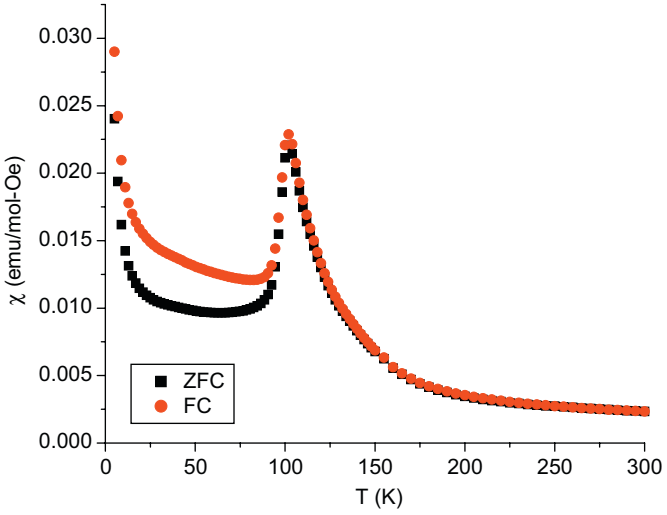

Fig. 4. ZFC and FC molar susceptibility data as a function of temperature. Note the sharp maximum near 110 K.

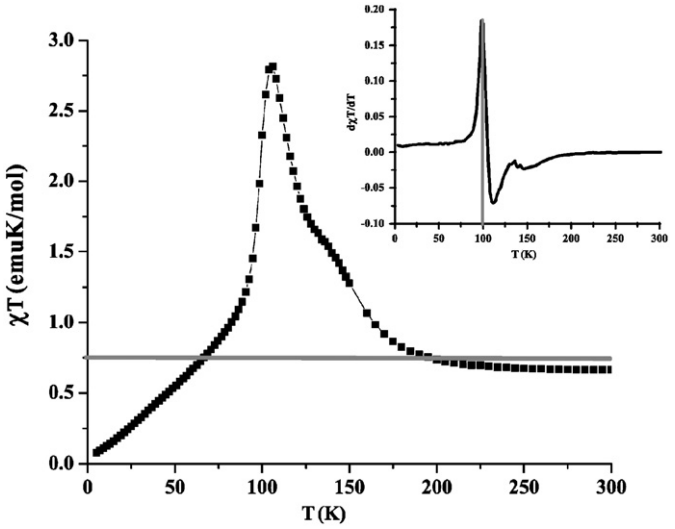

Fig. 5. χT as a function of temperature. The horizontal line shows the calculated spin-only Curie constant. The inset shows the Fisher heat capacity [29] in which the transition temperature is marked by a vertical line.

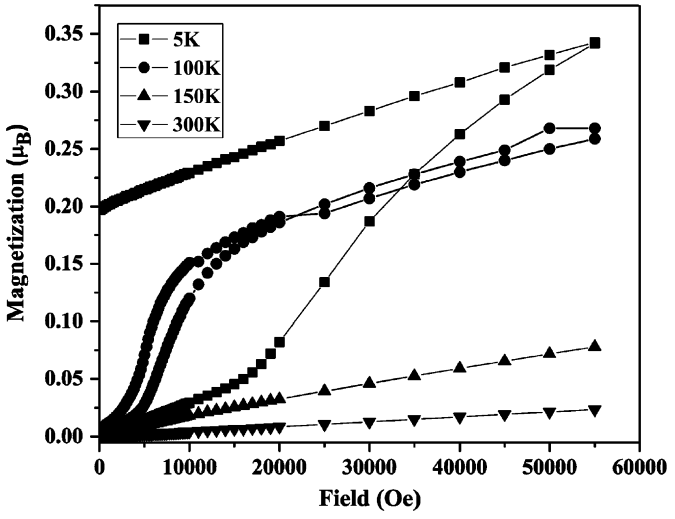

Fig. 6. The isothermal magnetization vs. applied field behavior. A hysteresis persists up to 100 K, and disappears at 150 K. Note the metamagnetic transitions for 100 and 5 K.

other pillared perovskite materials. Attempts to fit the high temperature data to the Curie–Weiss function were not successful as the parameters obtained depended strongly on the fitting range. It is concluded that the Curie–Weiss regime is not reached for this material below 300 K. Useful information can be obtained from a plot of χT vs. T for the ZFC data shown in Fig. 5. The horizontal line marks the calculated spin-only Curie constant, 0.75 emu/mol K, for two $S = \frac{1}{2}$ ions, appropriate for both Mo^{5+} and V^{4+}, per formula unit. As can be seen, the data approach this value as T approaches 300 K. The χT product exceeds the spin only, paramagnetic, value below about 175 K and reaches a maximum value at 110 K. This is taken as evidence for short-range ferrimagnetic correlations within the perovskite planes. Note also the shoulder near 150 K which might signal short-range intra-planar AF correlations. The sharp drop in χT below the maximum normally signals long-range AF coupling of ferrimagnetic layers. The critical temperature can be estimated from a plot of the so-called Fisher heat capacity, $d(\chi T)/dT$ vs. T shown in the inset which gives $T_c = 100$ K [29].

Isothermal magnetization data were also obtained (Fig. 6). The data at 5 K show a linear increase of magnetization up to ~1.7 T and then a rapid increase to reach $0.343\mu_B$ at 5.5 T. However, saturation is not achieved at this field. A hysteresis is present at 5 K and a remnant magnetization of $0.2\mu_B$ is observed. The data at 100 K follow a similar trend by a gradual upturn to 0.4 T followed by a rapid rise in magnetization. A clear hysteresis can also be observed at 100 K. The data at higher temperatures of 150 and 300 K are linear consistent with a typical paramagnetic system. The observation of a sharp increase in magnetization at low fields is a feature observed in layered materials with relatively weak inter-layer antiferromagnetic interactions. This behavior can be explained by a metamagnetic-like transition in which application of a magnetic field flips the antiferromagnetic spin alignment between the layers. In this powder sample the metamagnetic critical field can be estimated as ~1.7 T from the beginning of an upturn in the 5 K data, although single-crystal data would be needed to determine this value more precisely. The hysteresis observed in the isothermal magnetization data is an indication of a ferromagnetic component that can be attributed to the residual moment in the perovskite layers due to the ferrimagnetic order and possibly spin canting. In this material both the $M1$ and $M2$ sites are occupied by $S = \frac{1}{2}$ ions, so the net moment will be small and will depend on differences in g-factors and on the exact distribution of ions over the two sites, an issue which has been

discussed earlier. Note that a net moment of the magnitude seen here is perhaps best understood if one site is diluted by a diamagnetic component. Both the critical field for the metamagnetic transition and the saturation moment can be compared with corresponding values for $La_5Mo_4O_{16}$ which were obtained on single crystals [16]. For this material, at 5 K the saturation moment is $\sim 0.38\mu_B$ and the metamagnetic critical field appears to be ~ 1 T or 10^4 Oe, both values being similar to those found for $La_5Mo_{2.75}V_{1.25}O_{16}$.

The availability of a relatively large sample permitted neutron diffraction studies which allow a study of the magnetic structure of this material and for the first time for any Mo-based pillared perovskite. Given that the magnetic ions involved have $S = 1/2$ with small local magnetic moments and that the system is magnetically very dilute (two magnetic ions out of 25) the intensity of the magnetic peaks is expected to be very weak. Nonetheless, it was possible to identify two magnetic reflections from a comparison of data at 300 and 3.8 K (Fig. 7), at 24.99(1)° and 25.77(3)° which can be indexed as $(-1\ -11/2)/(-111/2)$, and $(1\ -11/2)/(111/2)$, respectively, consistent with the case of the Re-based materials [12,15,18]. A structure peak $(110)/(1\ -10)$ is also indexed. Due to the low intensity of the magnetic peaks and also overlap of the 24.99(1)° peak with a peak from the side product, a refinement of magnetic structure was not possible. However, the data are sufficient to propose a model magnetic structure by simulation and comparison of relative intensities. From the indices the ordering wave vector is $\mathbf{k} = (0\,0\,\frac{1}{2})$ which requires an inter-layer AF ordering. The intra-layer order may be ferro(F) or AF(ferrimagnetic). Simulations showed that only the AF intra-layer model resulted in intensities at the observed magnetic reflections. This is consistent with the results of a spin dimer calculation of the intra-planar exchange interactions which will be discussed in the next section.

Thus, the magnetic structure is one in which the moments on *M*1 and *M*2 show AF coupling within the layers, and AF coupling between the layers as well (Fig. 8) as has been found for the Re- and Os-based pillared perovskites. An estimate of the ordered moments can be obtained from fitting the magnetic and non-magnetic $(110)/(1\ -10)$ reflection to Gaussians and comparison with calculated values from simulations. The spin direction is taken as parallel to the *c*-axis as no $(0\,0\,\frac{1}{2})$ reflection was observed. Moments of $1\mu_B$ each were placed at the *M*1 and *M*2 sites and the magnetic intensities were calculated. The results are shown in Tables 5 and 6. The agreement is seen to be reasonable. Given the large uncertainties associated with the data, further efforts to refine to the model were considered unwarranted.

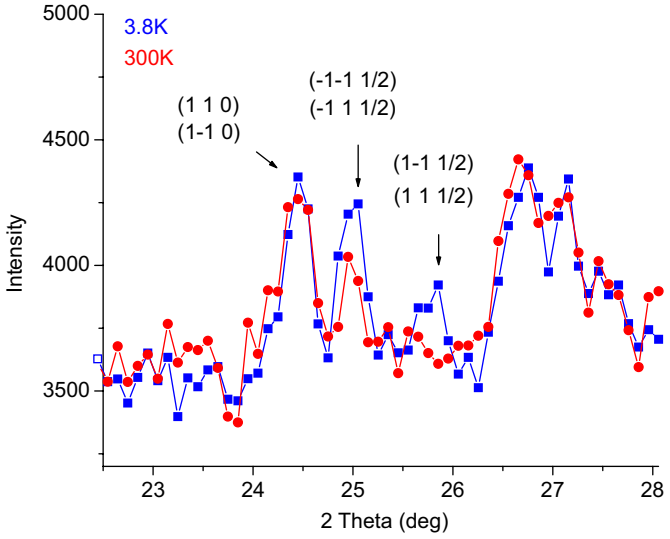

Fig. 7. Comparison of neutron diffraction data at 300 and 3.8 K. Magnetic reflections are indexed along with a pure crystal structure reflection.

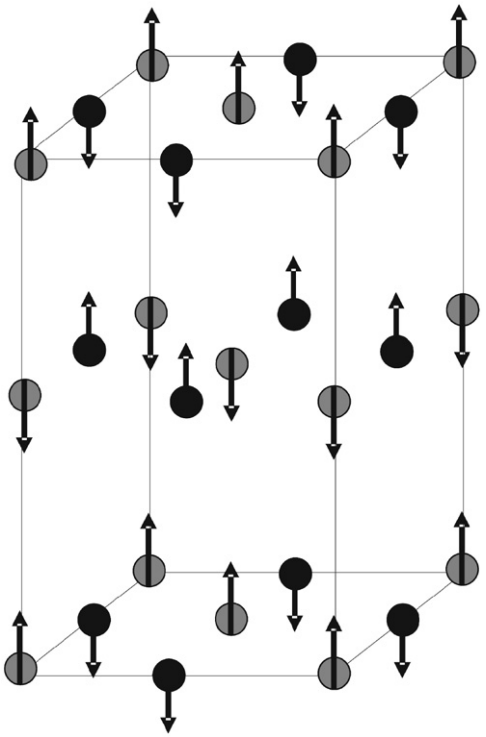

Fig. 8. The magnetic structure of $La_5Mo_{2.76(4)}V_{1.25(4)}O_{16}$. The grey and black circles represent *M*1 and *M*2 sites, respectively. The diamagnetic dimer sites are not shown. The long axis is the magnetic *c*-axis which equals $2c_{chem}$.

3.3. Tight binding, magnetic dimer model

The relative strengths of different possible spin interactions within the layers of this material were calculated. Fig. 2 illustrates these interaction pathways labled as J_1–J_4, the metal/metal distances for which are given in Table 5. In this material the d^1 ions Mo^{5+} and V^{4+} are responsible for the spin exchange interactions. From the results of Table 4, a psuedo-tetragonal compression is associated with both sites. This results in lifting the degeneracy of the t_{2g} orbitals by depressing the d_{xy} state compared to the d_{xz} and d_{yz} orbitals. The orbitals involved in the exchange are determined by the degree of the splitting. Two extreme cases can be considered. For a large splitting the single unpaired electron will reside exclusively in d_{xy} which is well separated from the other states. Consequently, only one orbital of each magnetic ion is involved in the spin exchange, and therefore there is only one interaction in each pathway for which Δe should be calculated. However, if the separation between these states is not significant, the occupation probability of d_{xz} and d_{yz} electron will be high, and these two orbitals will participate in spin interactions as well. At the other extreme, the probability that d_{xy}, d_{xz} and d_{yz} participate in the spin exchange will be the same, and the Δe resulting from each state should be taken into account. Therefore the intersite hopping energy will be given by the general formula

$$\langle(\Delta e)^2\rangle \approx \frac{1}{N^2}\sum_{\mu=1}^{N}(\Delta e_{\mu\mu})^2 \qquad (2)$$

Table 5
Observed intensities of magnetic and non-magnetic reflections for $La_5Mo_{2.76(4)}V_{1.25(4)}O_{16}$

(*h k l*)	3.8 K		300 K	
	Peak pos. (deg)	Int.	Peak pos. (deg)	Int.
(1 1 0)/(1 −1 0)	24.45(1)	267(22)	24.44(1)	267(30)
(−1 1 1/2)/(−1 −1 1/2)	24.99(1)	236(28)	24.99(1)	88(22)
(1 1 1/2)/(1 −1 1/2)	25.76(3)	140(37)	–	–

Table 6
Comparison of observed and calculated relative intensities for $La_5Mo_{2.76(4)}V_{1.25(4)}O_{16}$ assuming a model with 1 μ_B each on the *M*1 and *M*2 intra-planar sites and a moment direction parallel to the *c*-axis

(*h k l*)	3.8 K		3.8 K	
	Int. (Calc.)	Int. (Rel.)	Int. (obs.)	Int. (Rel.)
(1 1 0)	202			
(1 −1 0)	16			
Total	218	1	267(22)	1
(−1 −1 1/2)	68		236(28)	
(−1 1 1/2)	68		−88(22)	
Total	136	0.62	148(22)	0.55(11)
(1 1 1/2)	63			
(1 −1 1/2)	63			
Total	126	0.58	140(37)	0.52(11)

Table 7
Metal/metal distances for spin interaction within a perovskite-type layer

Exchange pathway	Distance (Å)
*M*1–*M*1 (J_1)	5.596
*M*2–*M*2 (J_2)	5.596
*M*1–*M*2 (1) (J_3)	3.953
*M*1–*M*2 (2) (J_4)	3.960

Table 8
Spin dimer analysis for the various exchange pathways identified in Fig. 2 for $La_5Mo_{2.76(4)}V_{1.25(4)}O_{16}$ assuming single occupation of d_{xy} and equal occupation of d_{xy},d_{xz} and d_{yz} orbitals

Pathway	Δe^2(meV)^2 (d_{xy})	Rel.	Δe^2(meV)^2 (d_{xy},d_{xz},d_{yz})	Rel.
J_1	1224	8.9×10^{-4}	1231	2.1×10^{-4}
J_2	616	4.5×10^{-4}	616	1.05×10^{-4}
J_3	1.33×10^{6}	0.97	5.83×10^{6}	0.98
J_4	1.37×10^{6}	1	5.96×10^{6}	1

where N is the number of orbitals and μ indicates each particular orbital participating in the interactions. Finally the obtained value for $\langle(\Delta e)^2\rangle$ will be used to determine the strengths of different interaction pathways according to

$$J = -2\frac{\langle(\Delta e)^2\rangle}{U} \quad (3)$$

A further assumption is that the inter-electron repulsion, U, will not be appreciably different for the two d^1 ions involved, Mo^{5+} and V^{4+}. While this is not strictly true, we note that this assumption will result in errors of at most a factor of two or so. Calculations were done for both extreme cases for the four pathways identified in Fig. 2, the interatomic distances for which are listed in Table 7. The calculated Δe values are listed in Table 8 and reveal that J_3 and J_4, corresponding to the two possible *M*1–*M*2 nearest-neighbor interactions along the $\langle 100\rangle$ and $\langle 010\rangle$ directions, are the strongest interactions by $\sim10^4$ over J_1 and J_2, which correspond to next nearest neighbor *M*1–*M*1 and *M*2–*M*2 interactions, respectively. The result is qualitatively the same for both extreme cases and by extension, any intermediate case. This is consistent with the magnetic structure found for this material that was discussed earlier, as large Δe values obtained by the extended Hückel, method indicate antiferromagnetic interaction of spins between the nearest neighbor *M*1 and *M*2 sites.

4. Conclusions

A new pillared perovskite compound containing an "early 3*d* transition element, $La_5Mo_{2.76(4)}V_{1.25(4)}O_{16}$, was synthesized by solid-state reaction, thus extending the crystal chemistry of this series. A structure refinement in *C*2/*m* using both X-ray and neutron diffraction data showed that within the perovskite layers, the *M*1 site has a mixed occupancy of Mo and V in the ratio Mo/V = 0.75/0.25, while the *M*2 is almost completely occupied by V. It is argued that the *M*1 site contains Mo^{5+} and V^{4+} while the *M*2 site is predominantly V^{4+}. A very short Mo–Mo distance of 2.46(2) Å is found in the dimeric edge-sharing units, indicating a Mo–Mo double bond between two $Mo^{4+}(4d^2)$ ions as seen in the related materials, $La_5Mo_4O_{16}$ and $La_5Mo_{3.31}Co_{.69}O_{15.8}$. Thus, the Mo1 sites do not contribute to the paramagnetic susceptibility. The bulk magnetic properties of this compound are similar to those of other pillared perovskites. Short-range intra-planar correlations set in below ~250 K, indeed, a pure Curie–Weiss regime is not found up to 300 K. The dominant short-range order is ferrimagnetic, causing an increase of the χT product with decreasing temperature to well above the spin-only value for two $S=\frac{1}{2}$ ions. Long-range order sets in below 100 K. Isothermal field sweeps give evidence for a metamagnetic critical field of ~1.7 T at 5 K. The magnetic structure of this material was determined from neutron diffraction data for the first time for any Mo-based pillared perovskite. The ordering wave vector is $\mathbf{k}=(00\frac{1}{2})$ and ferrimagnetically ordered layers of moments of $\sim1\mu_B$ each on the *M*1 and *M*2 sites are coupled antiferromagnetically between the layers. A theoretical study of spin interactions within the perovskite-type layers using extended Hückel, spin dimer analysis is consistent with the observed ferrimagnetic intra-planar spin correlations.

Acknowledgments

We acknowledge support for this work from the Natural Sciences and Engineering Research Council of Canada through a Discovery Grant to J.E.G. and MRS grants to the Canadian Neutron Beam Centre and the Brockhouse Institute for Materials Research.

Mr. Subrata Shaw carried out early work on the synthesis of this material.

References

[1] K.-I. Kobayashi, T. Kimura, H. Sawada, K. Terakura, Y. Tokura, Nature 395 (1998) 677.
[2] A.P. Ramirez, J. Phys.: Condens. Matter 9 (1997) 8171.
[3] T.H. Kim, M. Uehara, S.W. Cheong, S. Lee, Appl. Phys. Lett. 74 (1999) 1737.
[4] G.D. Tang, X.M. Liu, Z.Z. Li, D.L. Hou, X. Zhao, L.H. Liu, W.H. Qi, Y. Yu, R.C. Yu, C.Q. Jinphys, Stat. Sol. (a) 203 (2006) 2522.
[5] M.A. Basith, Sk. Manjura Hoque, Md. Shahparan, M.A. Hakim, M. Huq, Physica B 395 (2007) 126.
[6] M. Imada, A. Fujimori, Y. Tokura, Rev. Mod. Phys. 70 (1998) 1039.
[7] L.O.-S. Martin, J.P. Chapman, L. Lezama, J.S. Marcos, J. Rodríguez-Fernández, M.I. Arriortua, T. Rojo, Eur. J. Inorg. Chem. (2006) 1362–1370.
[8] W.H. McCarroll, C. Darling, G. Jakubicki, J. Solid State Chem. 48 (1983) 189.
[9] M. Ledesert, Ph. Labbe, W.H. McCarroll, H. Leligny, B. Raveau, J. Solid State Chem. 105 (1993) 143.

[10] C.R. Wiebe, A. Gourrier, T. Langet, J.F. Britten, J.E. Greedan, J. Solid State Chem. 151 (2000) 31.
[11] K.V. Ramanujachary, S.E. Lofland, W.H. McCarroll, T.J. Emge, M. Greenblatt, J. Solid State Chem. 164 (2002) 70.
[12] L. Chi, A.E.C. Green, R. Hammond, C.R. Wiebe, J.E. Greedan, J. Solid State Chem. 170 (2003) 165.
[13] L. Chi, I.P. Swainson, J.E. Greedan, J. Solid State Chem. 177 (2004) 3086.
[14] K.V. Ramanujachary, M. Greenblatt, W.H. McCarroll, J.B. Goodenough, Mater. Res. Bull. 28 (1993) 1257.
[15] A.E.C. Green, C.R. Wiebe, J.E. Greedan, Solid State Sci. 4 (2002) 305.
[16] S.E. Lofland, T. Scabarozi, K.V. Ramanujachary, W.H. McCarroll, J. Magn. Magn. Mater. 260 (2003) 184.
[17] S.E. Lofland, J. Hattrick-Simpers, K.V. Ramanujachary, W.H. McCarroll, J. Magn. Magn. Mater. 265 (2003) 113.
[18] H.L. Cuthbert, L. Cranswick, J.E. Greedan, J. Solid State Chem. 179 (2006) 1938.
[19] P.H. Hubert, P. Michel, C. Vincent, C. R. Acad. Sci. Ser. IIc 269 (1969) 1287.
[20] P.W. Selwood, Magnetochemistry, second ed., Interscience Publishers, Inc., New York, 1996.
[21] M.H. Whangbo, H.J. Koo, D.J. Dai, J. Solid State Chem. 176 (2003) 417.
[22] J. Ren, W. Liang, M.H. Whangbo, Crystal and Electronic Structure Analysis Using CAESAR, 〈http://www.primeC.com〉, 2005.
[23] E. Clementi, C. Roetti, At. Data Nucl. Data Tables 14 (1974) 177.
[24] A.D. McLean, R.S. Mclean, At. Data Nucl. Data Tables 26 (1981) 197.
[25] T. Roisnel, J. Rodriguez-Carvajal, FULLPROF ver 1.9c: Rietveld, Profile Matching & Integrated Intensity Refinement of X-ray and/or Neutron Data, Laboratoire Léon Brillouin, Saclay, France, 2001.
[26] T. Roisnel, J. Rodríguez-Carvajal, WinPLOTR: a Windows tool for powder diffraction patterns analysis, In: R. Delhez, E.J. Mittenmeijer (Eds.), Proceedings of the Seventh European Powder Diffraction Conference (EPDIC 7), Mater. Sci. Forum (2000) 118–123.
[27] I.D. Brown, D. Altermatt, Acta Crystallogr. B 41 (1985) 244.
[28] VALENCE program, 〈http://www.ccp14.ac.uk/ccp/web-mirrors/i_d_brown/〉.
[29] M.E. Fisher, Philos. Mag. 7 (1962) 1731.